Aberrant methylation-mediated decrease of lncRNA HNF1A-AS1 contributes to malignant progression of laryngeal squamous cell carcinoma via EMT

YEWEN SHI[1*], QINGQING ZHANG[1*], MENG XIE[1], YANI FENG[1], SIJING MA[1], CHUNXI YI[2], ZIHAN WANG[3], YANJU LI[4], XIAOHONG LIU[1], HAIQIN LIU[1], HUI YANG[1], YAN YAN[1], YITONG ZHANG[1], XIAOYONG REN[1] and HUANAN LUO[1]

[1]Department of Otorhinolaryngology Head and Neck Surgery, The Second Affiliated Hospital of Xi'an Jiaotong University; [2]Department of Otorhinolaryngology Head and Neck Surgery, Xi'an Central Hospital, Xi'an, Shaanxi 710004; [3]Department of Otorhinolaryngology Head and Neck Surgery, Xi'an Children's Hospital, Xi'an, Shaanxi 710003; [4]Department of Pathology, Yanan University Affiliated Hospital, Yan'an, Shaanxi 716000, P.R. China

Received March 28, 2020; Accepted August 24, 2020

DOI: 10.3892/or.2020.7823

Abstract. Aberrant methylation is one of the most frequent epigenetic alterations that regulate the expression levels of genes, including long non-coding RNAs (lncRNAs), in tumors. However, to the best of our knowledge, the expression and function of hepatic nuclear factor 1α antisense RNA 1 (HNF1A-AS1) and its methylation condition have not yet been reported in the development and progression of laryngeal squamous cell carcinoma (LSCC). In the present study, the expression and methylation of HNF1A-AS1 were first examined by reverse transcription-quantitative PCR, bisulfite genomic sequencing and methylation-specific polymerase chain reaction in samples from patients with LSCC, which were based on the *in silico* analysis using The Cancer Genome Atlas data, and were then further verified in LSCC cell lines with and without 5-Aza-2'-deoxycytidine (5-Aza-dC) treatment. Subsequently, proliferation, cell cycle distribution, migration and invasion of LSCC cells following either knockdown or overexpression of HNF1A-AS1 were determined *in vitro*. Furthermore, the characteristic of HNF1A-AS1 on epithelial-mesenchymal transition (EMT) changes was investigated *in vitro* and *in vivo*. The associations between the expression levels of HNF1A-AS1 and tumorigenicity and cervical lymph node metastasis were assessed in a xenograft model in nude mice. In the present study, downregulation and hypermethylation in CpG sites of HNF1A-AS1 were detected in LSCC tissues as well as metastatic cervical lymph nodes samples when compared with those in the adjacent non-tumor tissues. Additionally, HNF1A-AS1 inhibited proliferation, migration and invasion of LSCC cells *in vitro* by regulating the process of EMT. Furthermore, HNF1A-AS1 inhibited tumor growth and metastasis by regulating EMT *in vivo*. Additionally, the migration and invasion abilities, and the expression levels of HNF1A-AS1 and EMT markers in LSCC cells were significantly reversed by treatment with 5-Aza-dC. In summary, HNF1A-AS1 was downregulated by hypermethylation in LSCC and laryngeal cancer cells. These findings suggested that HNF1A-AS1 could serve as a tumor suppressor lncRNA in LSCC by regulating the EMT process, leading to the discovery of novel therapeutic targets and strategies for the treatment of patients with LSCC.

Correspondence to: Dr Xiaoyong Ren or Dr Huanan Luo, Department of Otorhinolaryngology Head and Neck Surgery, The Second Affiliated Hospital of Xi'an Jiaotong University, 157 Xiwu Road, Xi'an, Shaanxi 710004, P.R. China
E-mail: cor_renxiaoyong@126.com
E-mail: luohuanan@126.com

*Contributed equally

Abbreviations: LSCC, laryngeal squamous cell carcinoma; EMT, epithelial-mesenchymal transition; lncRNA, long non-coding RNA; HNF1A, hepatic nuclear factor 1α; HNF1A-AS1, HNF1A antisense RNA 1; IHC, immunohistochemical; IHS, immunohistochemical scores; 5-Aza-dC, 5-Aza-2'-deoxycytidine; MSP, methylation-specific polymerase chain reaction; BSP, bisulfite genomic sequencing

Key words: lncRNA HNF1A-AS1, LSCC, methylation, EMT, invasion

Introduction

Laryngeal squamous cell carcinoma (LSCC) accounts for ~90% of all laryngeal malignancies, and has the second highest incidence among all types of head and neck squamous cell carcinoma (HNSCC) (1,2). The early symptoms of LSCC, such as hoarseness, dysphagia and cervical lymph node metastasis, are common and may be easily ignored (3). Over the past 10 years, the treatment modalities for LSCC have changed, including surgery and chemotherapy, but the prognosis still remains poor due to its uncontrolled invasion and metastasis (4,5). Therefore, it is crucial to understand the underlying

molecular mechanisms of LSCC invasion and metastasis in order to improve the therapy and overall prognosis of this disease.

Cancer cell invasion and metastasis are complex processes that involve several factors. One of the most critical molecular mechanisms that mediate the metastatic cascade in cancer cells is the epithelial-mesenchymal transition (EMT) (6). It is characterized by decreased E-cadherin expression and increased expression levels of nonepithelial cadherins, such as N-cadherin, and these are considered to be important hallmark changes. Notably, loss of E-cadherin expression is a rate-limiting step in the progression of a well-differentiated cancer to invasive carcinoma (7,8).

According to accumulating evidence, long non-coding RNAs (lncRNAs) are a large class of transcripts that are longer than 200 nucleotides without protein-coding potential, and exhibit close association with the occurrence, development and metastasis of human cancers, including LSCC (9-13). Hepatic nuclear factor 1α (HNF1A) antisense RNA 1 (HNF1A-AS1) is a natural antisense transcript of the HNF1A gene, and its start site is ~5 kb downstream of HNF1A. It is a newly identified lncRNA located at chromosomal band 12q24.31 with a length of 2,455 nucleotides (14,15). HNF1A-AS1 was initially identified in the regulation of proliferation and migration of esophageal adenocarcinoma cells (14). Furthermore, HNF1A-AS1 is downregulated in both gastric cancer tissues and cell lines (15). These findings indicate that HNF1A-AS1 may be involved in the suppression of gastric cancer occurrence and development (15). Furthermore, in a recent study, HNF1A-AS1 was demonstrated to be transcriptionally activated by HNF1α, inhibited the malignant properties of hepatocellular carcinoma cells both *in vitro* and *in vivo*, and contributed to the antitumor effects of HNF1α by directly regulating the enzyme activity of Src homology region 2 domain-containing phosphatase 1 (16). These results suggest that HNF1A-AS1 dysregulation serves an important role in carcinogenesis. Additionally, previous studies have revealed that the promoter regions of lncRNAs are subjected to DNA methylation-mediated epigenetic alterations during tumorigenesis in a number of types of cancer (17,18). However, to the best of our knowledge, the expression and function of HNF1-AS1, and its methylation condition, have not been reported in the development and progression of LSCC.

In the present study, the epigenetic downregulation of HNF1A-AS1 due to promoter hypermethylation in LSCC was demonstrated and its biological function was evaluated. The negative association of HNF1A-AS1 with EMT and inhibition of tumor invasion and metastasis in LSCC were observed.

Materials and methods

Clinical samples. A total of 30 patients (age range, 47-75 years; mean age, 61.31±7.0 years; female, 6.67%; male, 93.33%) diagnosed with LSCC and cervical lymph node metastasis at the Second Affiliated Hospital of Xi'an Jiaotong University (Xi'an, China) between January 2015 and December 2016 were enrolled in the present study. All patients provided written informed consent, and the present study was approved by the Ethics Committee of the Second Affiliated Hospital of Xi'an Jiaotong University. Samples were collected from the patients who underwent resection (partial laryngectomy or total laryngectomy), apart from those whose pathology types were not squamous cell carcinoma. Patients who only underwent biopsy without resection were excluded from the present study. Patients who received radiation or chemotherapy before surgery were also excluded. Pairs of laryngeal carcinoma tissues, adjacent non-tumor tissues (normal tissue was obtained 1.0 cm from tumor edge) and metastatic cervical lymph nodes were either fixed in 10% formalin at room temperature for 12-24 h or frozen in liquid nitrogen at -196˚C after surgical resection till use.

Cell culture and treatment. The human LSCC TU-686 (Procell Life Science & Technology Co., Ltd.), AMC-HN-8 (BeNa Culture Collection; Beijing Beina Chunglian Biotechnology Research Institute), TU-177 (Jennio Biotech Co., Ltd.) and 293T (Procell Life Science & Technology Co., Ltd.) cell lines were cultured in DMEM (Thermo Fisher Scientific, Inc.) supplemented with 10% FBS (HyClone; Cytiva) and 50 U/ml penicillin-streptomycin at 37˚C in a humidified atmosphere of 5% CO_2. Furthermore, the aforementioned cell lines were treated with different concentrations (0, 1, 2.5, 5 and 10 μM) of 5-Aza-2'-deoxycytidine (5-Aza-dC; cat. no. S3196; Selleck Chemicals) for 24, 48 and 72 h at 37˚C. Different concentrations of 5-Aza-dC were added to DMEM for treatments.

Transfection of cell lines. To generate lentiviruses that overexpress and target short hairpin RNA (shRNA) expression of HNF1A-AS1, a full-length cDNA of HNF1A-AS1 and oligonucleotides that encode HNF1A-AS1 shRNAs [shRNA-non-specific control (NC), shRNA-853, shRNA-1525 and shRNA-2048; Table SI] which were designed by Shanghai GenePharma Co., Ltd. and named according to the catalogue number were cloned into the pLVX-mCMV-ZsGreen-PGK-Puro vector or the pLVX-shRNA2-Puro vector (Biowit Technologies, Ltd.), respectively. All vectors were verified by Sanger sequencing (19). The lentiviral vectors were transfected into sub-confluent 293T cells together with packaging plasmid and envelope plasmid (Biowit Technologies, Ltd.) using Lipofectamine 2000 reagent (Invitrogen; Thermo Fisher Scientific, Inc.) to produce lentiviral particles. The lentiviruses in the medium were collected 48 h later and were concentrated by ultracentrifugation at 448 x g for 10 min at room temperature. The target cells (cultured in 6-cm plate) were infected by removing the old culture medium and replacing it with 0.5 ml diluted viral supernatant (MOI, 20). A total of 0.5 ml complete medium with Polybrene was added to each well. The plates were placed in a 37˚C incubator with 5% CO_2. Fresh media were added at 24 h after infection. Following another incubation for 48 h, puromycin (1 μg/ml) selection of stably transduced cells was started. Then, GFP-positive cells were sorted by flow cytometry. Cells were suspended in PBS at $1x10^7$ cells/ml and filtered prior to sorting by FACSAria II (BD Biosciences). FACSDiva software (version 6.1.3; BD Biosciences) was installed on the FACSAria II to operate the instrument and analyze the measurements.

Reverse transcription-quantitative PCR (RT-qPCR). RT-qPCR was used to detect the expression levels of HNF1A-AS1 (*Homo sapiens*; Table SI) in the clinical specimens and cultured

cell lines (cat. no. 9108/9109, RNAiso Plus, total RNA extraction reagent for RNA extraction; cat. no. RR036A, PrimeScript™ RT Master Mix, Perfect Real Time for reverse transcription; cat. no. RR820A, TB Green™ Premix Ex Taq™ II, Tli RNaseH Plus for RT-PCR; Takara Bio, Inc.). Reverse transcription was performed at 37˚C for 15 min followed by 85˚C for 5 sec and 4˚C hold. The RT-qPCR thermocycling conditions were as follows: Initial denaturation at 95˚C for 30 sec; 40 cycles of denaturation at 95˚C for 5 sec, and annealing and elongation at 60˚C for 30 sec; final extension 72˚C for 15 min (20,21). β-actin was used as the reference gene (forward, 5'-AGCGAG CATCCCCCAAAGTT-3'; reverse, 5'-GGGCACGAAGGC TCATCATT-3'). The relative expression levels of HNF1A-AS1 in each group (fold change compared with the control group) was calculated using the following formula: $RQ=2^{-\Delta\Delta Cq}$ (22). Each reaction was performed in triplicate.

Immunohistochemical (IHC) staining and immunofluorescence staining. The expression levels of E-cadherin (cat. no. ab1416; mouse; dilution, 1:500; Abcam), N-cadherin (cat. no. ab76057; rabbit; dilution, 1:500; Abcam), Vimentin (cat. no. ab92547; rabbit; dilution, 1:300; Abcam), Snail (cat. no. ab53519; goat; dilution, 1:100; Abcam) and Slug (Snail2; cat. no. 12129-1-AP; rabbit; dilution, 1:100; ProteinTech Group, Inc.) in clinical specimens and cultured cell lines were detected by IHC. Tissues were fixed in 10% neutral-buffered formalin at room temperature for 24 h and embedded in paraffin. Sections (4-μm thick) were deparaffinized in four changes of xylene for 5 min each. Sections were hydrated in 100, 90 and 80% ethanol for 5 min each. Subsequently, sections were rinsed in water. Antigens were retrieved with citrate buffer (cat. no. C9999; Sigma-Aldrich; Merck KGaA) and sections were microwaved for 15 min at 95˚C. Sections were blocked with 5% BSA (cat. no. A3059; Sigma-Aldrich; Merck KGaA) in PBS containing 0.1% Tween-20 (cat. no. 85114; Thermo Fisher Scientific, Inc.) for 1 h at room temperature. Sections were incubated with the aforementioned primary antibodies at 4˚C overnight. Sections were incubated with the secondary HRP antibody (dilution, 1:1,000; cat. nos. P0449, K4001 and K4003; Dako; Agilent Technologies, Inc.) for 1 h at room temperature. Images were captured under a light microscope (IX51; Olympus Corporation). Immunoreactivity was scored based on the number of positive cells and staining intensity, using Image-Pro Plus 6.0 software (Media Cybernetics, Inc.). Immunohistochemical scores (IHS) were determined by multiplying the quantity and staining intensity scores as follows: i) The quantity was rated on a scale of 0-4: 0, no staining; 1, <10% of cells stained; 2, 10-50% of cells stained; 3, 51-80% of cells stained; and 4, 81-100% of cells stained; and ii) staining intensity was rated on a scale of 0-3: 0, negative; 1, weak; 2, moderate; and 3, strong. Theoretically, the scores could range between 0 and 12. An IHS of 9-12 was considered strong immunoreactivity, 5-8 was considered moderate, 1-4 was considered weak, and 0 was considered negative (23). Immunofluorescence staining was performed as previously described (24).

Cultured cells were grown on cover slips or chamber slides. Culture media were removed and cells were rinsed with PBS. The cells were fixed with 4% formaldehyde for 15 min at room temperature. Sections were blocked with 5% BSA (cat. no. A3059; Sigma-Aldrich; Merck KGaA) in PBS containing 0.1% Triton™ X-100 (cat. no. 85111; Thermo Fisher Scientific, Inc.) for 1 h at room temperature. Cells were incubated with the primary antibodies at the aforementioned concentrations overnight at 4˚C in the dark. Sections were incubated with the secondary Cy5-conjugated antibody (dilution, 1:500; cat. nos. BA1031 and BA1032; Boster Biological Technology) for 1 h at room temperature in the dark. Sections were mounted with Prolong Gold medium-DAPI (cat. no. P36931; Invitrogen; Thermo Fisher Scientific, Inc.). Images were captured under a fluorescence microscope (IX51; Olympus Corporation).

Western blotting. The proteins were extracted using a RIPA buffer kit (cat. no. P0013B; Beyotime Institute of Biotechnology). Protein concentration was determined using a BCA protein concentration determination kit (cat. no. P0010; Beyotime Institute of Biotechnology). Protein (20 μg/lane) was loaded onto an SDS-PAGE precast gel (8-16%; cat. no. P0058B; Beyotime Institute of Biotechnology). The proteins were transferred to a nitrocellulose membrane (cat. no. 88018; Thermo Fisher Scientific, Inc.). Membranes were blocked with 5% BSA (cat. no. A3059; Sigma-Aldrich; Merck KGaA) in TBS with 0.1% Tween-20 (cat. no. 85114; Thermo Fisher Scientific, Inc.) for 1 h at room temperature. The proteins were assessed by incubation with the specific primary antibodies, including E-cadherin, Snail1, Vimentin and N-cadherin (all diluted 1:1,000), as well as Slug (cat. no. 9585; rabbit; dilution, 1:800; Cell Signaling Technology, Inc.), CyclinD1 (cat. no. 55506; rabbit; dilution, 1:1,000; Cell Signaling Technology, Inc.), proliferating cell nuclear antigen (PCNA; cat. no. 13110; rabbit; dilution, 1:1,000; Cell Signaling Technology, Inc.) and GADPH (cat. no. 10494-1-AP; rabbit; dilution, 1:1,000; ProteinTech Group, Inc.) overnight at 4˚C. Sections were incubated with the secondary HRP antibodies (dilution, 1:5,000; cat. no. BA1051, BA1060 and BA1054; Boster Biological Technology) for 1 h at room temperature. The membranes were visualized using a ChemiDoc MP system (Bio-Rad Laboratories, Inc.) with ECL substrate (EMD Millipore). Densitometric semi-quantification of the bands was performed using ImageJ software (v. 1.52n; National Institutes of Health).

Cell proliferation assays. Cell proliferation capacities were evaluated using a Cell Counting Kit-8 assay (Beyotime Institute of Biotechnology) according to the manufacturer's protocol. The results were plotted as mean ± SE of three separate experiments for each experimental condition.

Flow cytometry analysis of the cell cycle. The cell cycle analysis was performed using a Cell Cycle Staining kit [cat. no. CCS012; PI staining; Hangzhou Multi Sciences (Lianke) Biotech Co., Ltd.], and analyzed by flow cytometry (FACScan®; BD Biosciences) with CellQuest software (version 5.2.1; BD Biosciences). The ratios of cells in the G_0/G_1, S and G_2/M phases were calculated and compared with those in the control groups.

Cell migration and invasion assays. The cell migration ability was measured by scratch assay analysis with 100% confluence after starving cells in media containing 0.1% FBS overnight.

A 20-μl pipette tip was used to create the scratch. Then, the cells were cultured in the medium with a reduced concentration (1%) of serum to control for the influence of proliferation and avoid apoptosis for 0 (baseline), 24 and 48 h, and then the images of the same view were captured (light microscope; IX51; Olympus Corporation). ImageJ software was used to measure the wound area at different time points. The width of the wound divided by the width of the background field was used to calculate changes over time. The cell invasion ability was assessed using 6.5-mm Transwell chambers (Corning Inc.) Matrigel was thawed for 24 h in ice at 4˚C in a refrigerator. A total of 100 μl Matrigel (0.4 mg/ml) was loaded into the upper chamber and incubated for 24 h at 4˚C in a CO_2 incubator. After 24 h, 750 μl DMEM complete medium with 10% FBS was added into the lower chamber. In the upper chamber, 200 μl cell suspension ($2x10^5$ cells/ml in only DMEM) was added onto the Matrigel-coated cell culture insert and incubated for 24 h. After 24 h, the medium in the upper chamber was removed, followed by washing with PBS. Cells were fixed with 4% formaldehyde for 30 min at room temperature and stained with 0.4% crystal violet for 10 min at room temperature. Non-invaded cells were removed with cotton swabs. Invasive cells were counted in four random microscopic fields (light microscope; IX51; Olympus Corporation). Each assay was performed in triplicate.

Analysis of CpG islands in the promoter of HNF1A-AS1. The UCSC genome browser public database (http://genome.ucsc.edu) and Methprimer 1.0 (http://www.urogene.org/methprimer/) tools were used to identify the CpG islands of HNF1A-AS1 (2 kb upstream of the transcriptional start site) (25). The prediction of CpG islands was performed using the following parameters: >100 bp window, percentage of C plus G >50%, and observed/expected CpG ratio >0.6. Since the number of patients with LSCC in The Cancer Genome Atlas (https://portal.gdc.cancer.gov/) database was not sufficient, 530 patients with head and neck squamous cell carcinoma included in the TCGA HNSC cohort were analyzed retrospectively (26).

Methylation-specific polymerase chain reaction (MSP) and bisulfite genomic sequencing (BSP). Total DNA was extracted from cell lines and tissue specimens using the MiniBEST Genomic DNA Extraction kit (cat. no. 9765; Takara Bio, Inc.). The EZ DNA Methylation-Gold kit (Zymo Research Corp.) was used for converting bisulfate for subsequent methylation analysis. The primers used for MSP and BSP were complementary to the promoter regions of HNF1A-AS1 (Table SI). The bisulphate-modified DNA was used as template for amplification in MSP detection (cat. no. R110A; Takara Bio, Inc.; methylated: 98˚C for 10 sec, 61.3˚C for 5 sec and 72˚C for 30 sec, 40 cycles; unmethylated: 98˚C for 10 sec, 58.1˚C for 5 sec and 72˚C for 30 sec, 40 cycles), and the PCR products were subjected to 1.5% agarose (cat. no. AG006; Canvax Biotech) gel electrophoresis (100 V; 40 min). Tris-Acetate-EDTA buffer was used in the preparation and running of the gel, and 10 μl GelRed (cat. no. 41003-T; Biotium, Inc.) was added to 100 ml agarose gel. Subsequently, 6 μl sample (5 μl and 1 μl 6X DNA loading buffer; cat. no. R0611; Thermo Fisher Scientific, Inc.) per lane was loaded on an agarose gel. The Gel Doc EZ imaging system (Bio-Rad Laboratories, Inc.) came equipped with Image Lab™ software version 3.0, with auto image capture and auto analysis, and was used for semi-quantification. Additionally, the modified DNA was amplified, purified, subcloned into pMD19-T vector (Takara Bio, Inc.) and transformed into *E. coli* (DH5-alpha; Biowit Technologies, Ltd.), cultured in Luria broth medium (LB; cat. no. 10855001; Thermo Fisher Scientific, Inc.) with 50 μg/ml ampicillin at 37˚C with 0.04% CO_2, according to the manufacturer's protocol. Finally, five isolated colonies that were grown on LB agar plates (Thermo Fisher Scientific, Inc.) containing ampicillin with X-gal (0.2 mg/ml)/IPTG (1 mM) were picked, and underwent sequencing and analysis using an ABI 3730 DNA Sequencer (Applied Biosystems; Thermo Fisher Scientific, Inc.) for BSP detection.

In vivo xenograft tumorigenicity, tumor invasion and cervical lymph node metastasis assays. Briefly, 8-week-old male Bal/Bc nude mice (n=44; weight, 22.95±0.41 g) were supplied by the Institute of Zoology, Xi'an Jiaotong University Health Science Center (Xi'an, China). The animals were fed and raised in an ultraclean specific-pathogen-free laminar flow rack with a constant temperature (20-26˚C), humidity (40-50%) and 12/12-h light/dark cycle. Food and fresh water were accessible at all times. All animal experiments were performed according to the Guide for the Care and Use of Laboratory Animals of the National Institutes of Health (27) and were authorized by the Medical Ethics Committee of Xi'an Jiaotong University. Animal experiments were performed in May 2018.

For *in vivo* tumorigenicity experiments, DMEM without FBS and Matrigel (cat. no. 356234; BD Biosciences) were mixed 1:1 as resuspension solution. The cells (TU-686/shRNA-2048, TU-177/HNF1A-AS1 and control cells;100 μl; $1x10^6$) were subcutaneously injected into the right flank of each mouse (five mice per group). The mice were monitored for weight, respiration, ability to ambulate, taking food, drinking, tumor size, ulceration, infection, and necrosis by a specialized technician at the animal facility. The tumor volume of each mouse was determined by measuring two of its dimensions and calculated using the following formula: Tumor volume=length x width^2/2. The humane endpoints included a rapid weight loss of 15% within a few days and a tumor diameter >1.5 cm (subcutaneous xenografts) in any single dimension. Body weights of mice are shown in Fig. S1A and B. Tumor-bearing mice were euthanized using CO_2 (20% of the volume of the chamber per min). The time interval between injection and euthanasia was 43 days.

For *in vivo* tumor cervical lymph node metastasis, the present study used an orthotopic xenograft model of head and neck cancers as described previously (28,29). The indicated cells (TU-686/shRNA-2048, TU-177/HNF1A-AS1 and control cells; 30 μl; $2x10^5$) (28,29) were injected submucosally into the tongue of nude mice (6 mice per group) (30). The resuspension solution was the same as for flank injection. Tumor-bearing mice were euthanized by CO_2 (20% of the volume of the chamber per min). The time interval between injection and euthanasia was 21 days. Finally, submucosal tongue tumors and cervical lymph nodes were surgically excised, weighed and imaged. Pathological examinations of cervical lymph nodes were performed to confirm metastasis.

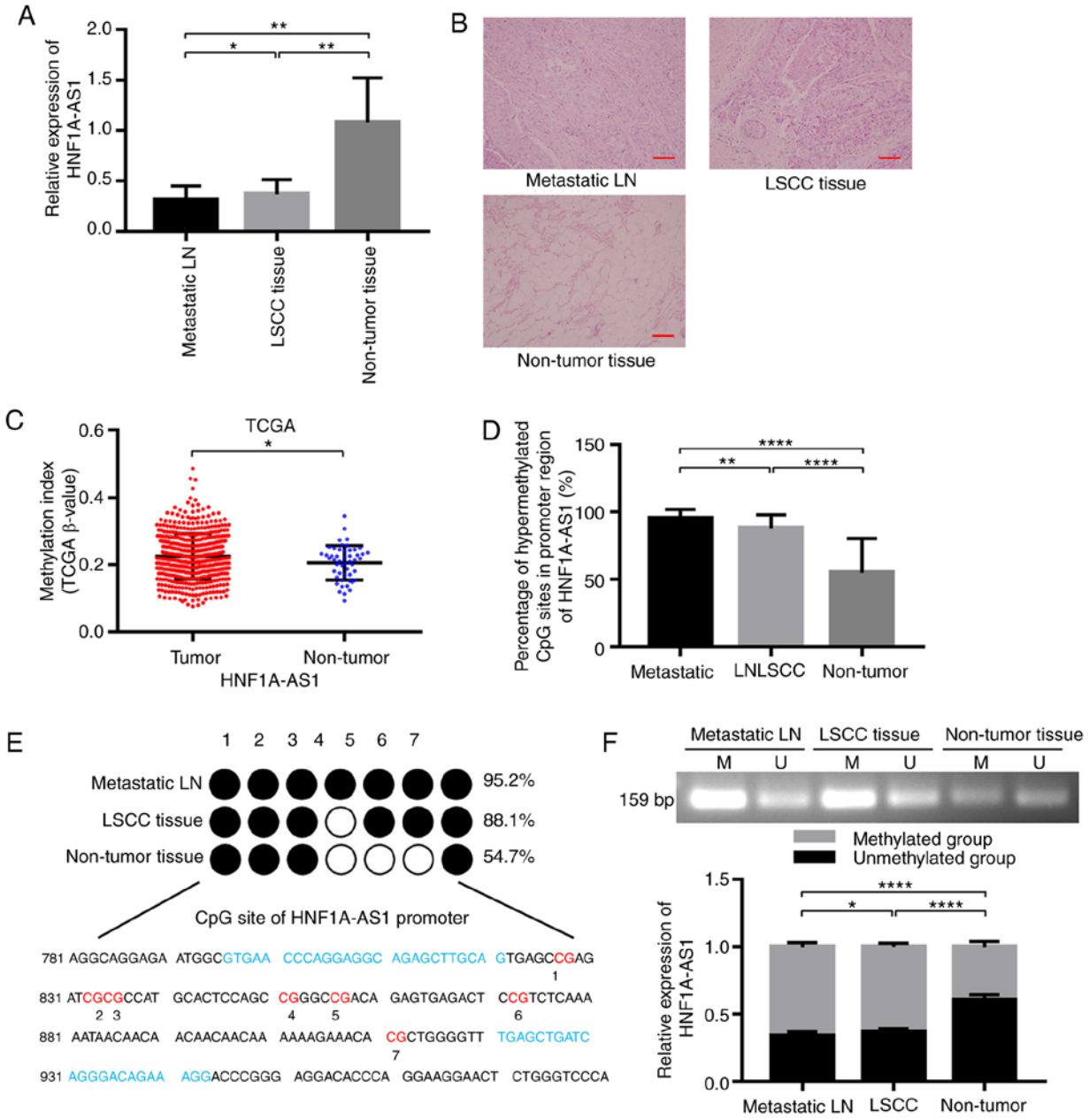

Figure 1. HNF1A-AS1 is downregulated and hypermethylated in LSCC tissues and metastatic cervical lymph nodes. (A) Expression levels of HNF1A-AS1 in primary LSCC tissues, adjacent metastatic lymph nodes samples and non-tumor tissues were examined by reverse transcription-quantitative PCR. GAPDH was used as an internal control (n=30). (B) Representative HE staining in primary LSCC tissues, adjacent non-tumor tissues and metastatic cervical lymph nodes of patients with LSCC. Scale bar, 50 μm. (C) Percentage methylation of HNF1A-AS1 was analyzed in tissues from 530 patients with head and neck squamous cell carcinoma and 50 normal adjacent tissues included in TCGA. (E) Bisulfite genomic sequencing was performed to examine the methylation status of the HNF1A-AS1 promoter region in primary LSCC tissues, metastatic cervical lymph nodes and adjacent non-tumor tissues from 30 patients, and (D) methylation status was analyzed statistically. (F) The methylation status of the CpG island in the HNF1A-AS1 promoter was determined by methylation-specific polymerase chain reaction assays in primary LSCC tissues, metastatic cervical lymph nodes and adjacent non-tumor tissues from 30 patients. For statistical analysis, one-way ANOVA with Tukey's post hoc test was used for data in (A, D and F) and an unpaired t-test was used for data in (C) Data are presented as the mean ± SD. All assays were performed in triplicate, and the values represent the mean of three independent experiments. *P<0.05, **P<0.01 and ****P<0.0001. HNF1A-AS1, hepatic nuclear factor 1 α antisense RNA 1; LN, lymph node; LSCC, laryngeal squamous cell carcinoma; TCGA, The Cancer Genome Atlas.

Statistical analysis. Statistical analysis was performed using SPSS v19.0 (IBM Corp.) and GraphPad Prism 5.0 (GraphPad Software, Inc.). All data are presented as the mean ± SD. *In vitro* experiments were performed in triplicate. An unpaired two-tailed Student's t-test, one-way ANOVA with Tukey's post hoc test and the χ^2 test were used to analyze the data. P<0.05 was considered to indicate a statistically significant difference.

Results

HNF1A-AS1 expression is downregulated in LSCC tissues and metastatic cervical lymph nodes. The results of RT-qPCR demonstrated that the expression levels of HNF1A-AS1 were significantly downregulated in LSCC tissues and metastatic lymph node samples compared with in the adjacent non-tumor tissues (P<0.05; Fig. 1A). The results of HE staining are shown

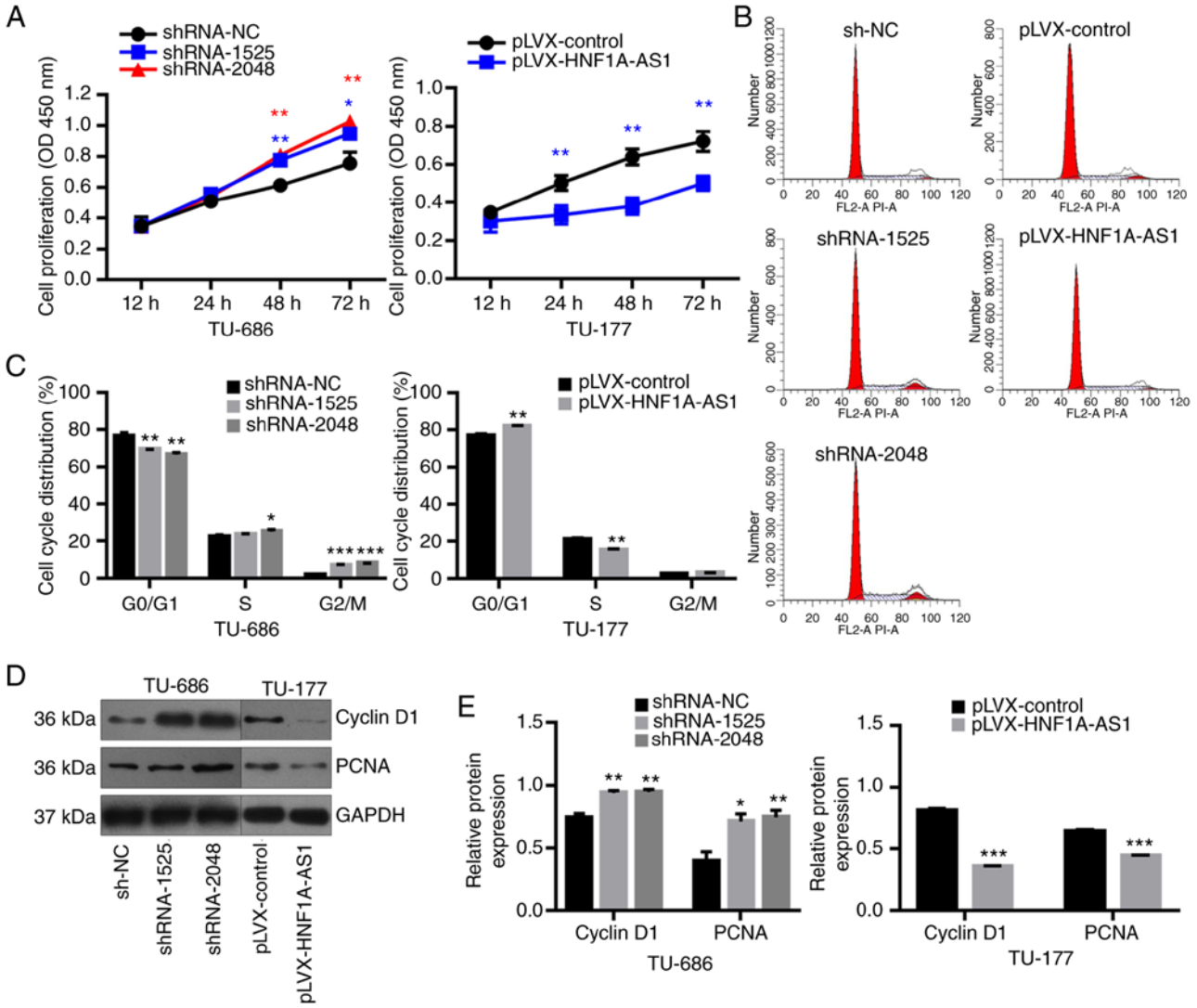

Figure 2. HNF1A-AS1 inhibits cell proliferation and cell cycle progression in laryngeal cancer cells. (A) Cell proliferation was assessed at 12, 24, 48 and 72 h using a Cell Counting Kit-8 assay. (B) Cell cycle distribution was analyzed by flow cytometry and (C) results of cell cycle analysis were analyzed statistically. (D) Western blotting was used to evaluate the protein expression levels of Cyclin D1 and PCNA following transfection of sh-NC, shRNA-1525 or shRNA-2048 into TU-686 cells and pLVX-control or pLVX-HNF1A-AS1 into TU-177 cells and (E) results of western blotting were analyzed statistically. Data are presented as the mean ± SD. All assays were performed in triplicate, and the values represent the mean of three independent experiments. For statistical analysis, ANOVA with Tukey's post hoc test was used to compare the sh-NC, shRNA-1525 and shRNA-2048 groups, and an unpaired t-test was used to compare the pLVX-control and pLVX-HNF1A-AS1 groups. *P<0.05, **P<0.01, ***P<0.001. HNF1A-AS1, hepatic nuclear factor 1 α antisense RNA 1; NC, negative control; PCNA, proliferating cell nuclear antigen; shRNA, short hairpin RNA.

in Fig. 1B. It was demonstrated that the downregulation of HNF1A-AS1 may serve an important role in the development and progression of LSCC.

Methylation analysis of the HNF1A-AS1 promoter in vivo. To further ascertain whether the downregulation of HNF1A-AS1 expression was caused by promoter hypermethylation in primary LSCC, the methylation frequency in the promoter region of HNF1A-AS1 in HNSCC tissues and metastatic cervical lymph nodes was examined and was significantly higher than that in the corresponding normal tissues according to the TCGA database (Fig. 1C).

Furthermore, the methylation status of HNF1A-AS1 in 30 paired tissues in patients was analyzed using BSP, CpG methylation of HNF1A-AS1 promoter was detected in all primary LSCC tissues (88.1%) and metastatic cervical lymph nodes (95.2%), and the results revealed significantly lower methylation in the matched normal adjacent tissues (54.7%; Fig. 1D and E). Similar to the BSP results, apparent methylation of HNF1A-AS1 in the promoter region was also detected to be higher in primary LSCC tissues and metastatic cervical lymph nodes than normal adjacent tissues by MSP (Fig. 1F). These results implied that hypermethylation of CpG islands in the promoter region was the major regulatory mechanism of HNF1A-AS1 downregulation in LSCC.

HNF1A-AS1 inhibits cell proliferation and cell cycle in laryngeal cancer cells. Compared with HNF1A-AS1 expression in AMC-HN-8 cells, its expression was high in the TU-686 cell line, but was decreased in the TU-177 cell line as demonstrated by RT-qPCR (P<0.01; Fig. S2A). Therefore, TU-686 and TU-177 cell lines were selected as research targets for

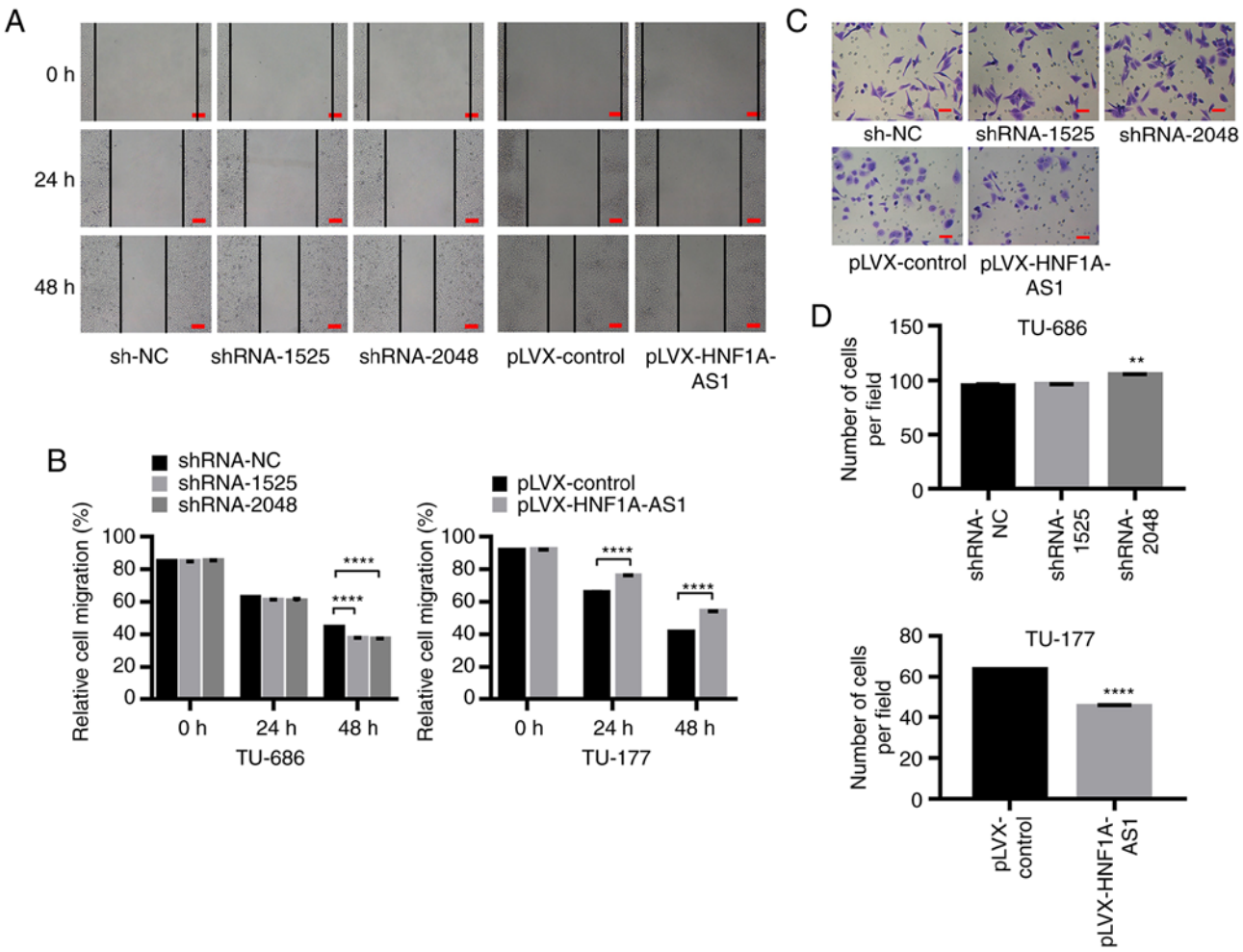

Figure 3. HNF1A-AS1 suppresses cell migration and invasion *in vitro*. (A) Migration of TU-686/shRNA-1525, TU-686/shRNA-2048, TU-177/HNF1A-AS1 and control cells was assessed using a scratch assay, and (B) results of migration were analyzed statistically. Scale bar, 100 μm. (C) Transwell invasion assays were performed to determine the invasive abilities of TU-686/shRNA-1525, TU-686/shRNA-2048, TU-177/HNF1A-AS1 and control cells, and (D) results of the Transwell invasion assay were analyzed statistically. Scale bar, 50 μm. For statistical analysis, ANOVA with Tukey's post hoc test was used to compare the sh-NC, shRNA-1525 and shRNA-2048 groups, and an unpaired t-test was used to compare the pLVX-control and pLVX-HNF1A-AS1 groups. Each experiment was performed in triplicates. **P<0.01, ****P<0.0001. HNF1A-AS1, hepatic nuclear factor 1 α antisense RNA 1; NC, negative control; shRNA, short hairpin RNA.

further functional studies. To downregulate the expression levels of HNF1A-AS1 endogenously in laryngeal cells, small shRNA-853, shRNA-1525 and shRNA-2048 were separately transfected into TU-686 cells and the interference effects were confirmed by RT-qPCR analysis. At 48 h post-transfection, the expression levels of HNF1A-AS1 were significantly decreased by shRNA-1525 (50%; P<0.01) and shRNA-2048 (75%; P<0.0001) compared with scrambled shRNA-NC (Fig. S2B). Furthermore, HNF1A-AS1 expression in TU-177 cells was upregulated 10 times following lentiviral vector transfection (pLVX-HNF1A-AS1 vs. pLVX-control; Fig. S2C). Considering the remarkable interference and overexpression effects of HNF1A-AS1, three stable cell lines (TU-686/shRNA-1525, TU-686/shRNA-2048 and TU-177/HNF1A-AS1) were used for subsequent experiments.

When compared with the negative control group, knockdown of HNF1A-AS1 resulted in a significant increase in cell proliferation in TU-686 cells at 48 and 72 h. Conversely, overexpression of HNF1A-AS1 decreased the cell proliferation in TU-177 cells at 24, 48 and 72 h (Fig. 2A). Additionally, the downregulation of HNF1A-AS1 promoted TU-686 cell transition from G_0/G_1 to S phase (Fig. 2B and C), but HNF1A-AS1 overexpression arrested cell cycle at G_0/G_1 phase (Fig. 2B and C). Furthermore, knockdown of HNF1A-AS1 in TU-686 cells significantly promoted the expression of cell cycle-related protein cyclin D1 and PCNA; however, these were inhibited by overexpression of HNF1A-AS1 in TU-177 cells (Fig. 2D and E). Overall, overexpression of HNF1A-AS1 could inhibit the proliferation of LSCC cells and this was partially accompanied by G_0/G_1 arrest.

HNF1A-AS1 inhibits cell migration and invasion, and reverses epithelial mesenchymal transition in vitro. The cell migratory abilities were investigated by scratch assay analysis and the results revealed that HNF1A-AS1 downregulation significantly enhanced the migratory abilities of LSCC cells (Fig. 3A and B). In addition, a Transwell invasion assay demonstrated that decreased expression of HNF1A-AS1 following transfection with TU-686/shRNA-2048 significantly enhanced the invasive capacity of TU-686 cells (105.1±0.4 vs. 94.8±1.2; P<0.01;

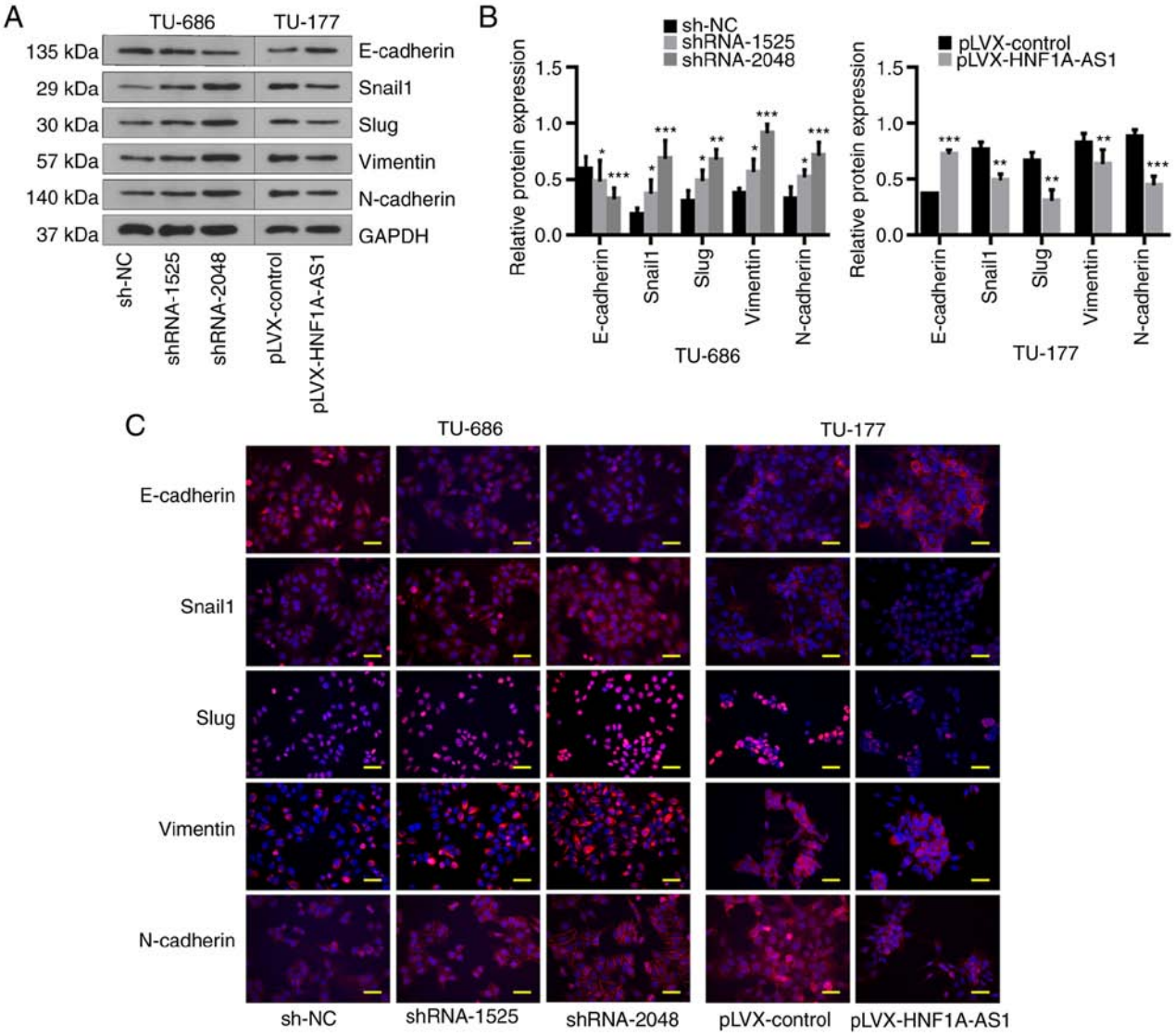

Figure 4. HNF1A-AS1 suppresses epithelial-mesenchymal transition *in vitro*. (A) Relative protein expression levels of E-cadherin, Snail1, Slug, Vimentin and N-cadherin were evaluated by western blot analysis in TU-686/shRNA-1525, TU-686/shRNA-2048, TU-177/HNF1A-AS1 and control cells, and (B) results of western blotting were analyzed statistically. (C) Analysis of E-cadherin, Snail1, Slug, Vimentin and N-cadherin expression (red) in TU-686/sh-NC, TU-686/shRNA-1525, TU-686/shRNA-2048, TU-177/HNF1A-AS1 and TU-177/HNF1A-AS1-NC cells by immunofluorescence. Blue DAPI staining shows the nuclei (DNA). Scale bar, 25 μm. Data are presented as the mean ± SD. All assays were performed in triplicate, and the values represent the mean of three independent experiments. For statistical analysis, ANOVA with Tukey's post hoc test was used to compare the sh-NC, shRNA-1525 and shRNA-2048 groups in (B), and an unpaired t-test was used to compare pLVX-control and pLVX-HNF1A-AS1 groups in (B). *P<0.05, **P<0.01, ***P<0.001. HNF1A-AS1, hepatic nuclear factor 1 α antisense RNA 1; NC, negative control; shRNA, short hairpin RNA.

Fig. 3C and D), whereas HNF1A-AS1 overexpression inhibited the invasive abilities of TU-177 cells (44.9±0.7 vs. 63.4±0.3; P<0.001; Fig. 3C and D). The expression levels of EMT-related markers were assessed as EMT serves a key role in tumor invasion and metastasis. The results of western blotting and immunofluorescence assays demonstrated that knockdown of HNF1A-AS1 notably downregulated E-cadherin expression and upregulated Snail1, Slug, Vimentin and N-cadherin expression, and vice versa when HNF1A-AS1 was overexpressed (Fig. 4). These data suggested that HNF1A-AS1 contributed to the invasion and metastasis of laryngeal cancer cells partly by affecting the EMT process.

HNF1A-AS1 suppresses tumor growth, EMT and lymph node metastasis in vivo. Xenograft tumor (subcutaneous) growth models revealed that tumor sizes were markedly increased following injection with TU-686/shRNA-2048 cells, while injection with TU-177/HNF1A-AS1 cells was associated with a reduction compared with the control group (Fig. 5A-C). The cervical lymph node metastasis model (submucosal injection in tongue) gave similar results to the xenograft subcutaneous model. Tumor weights were increased for injection with TU-686/shRNA-2048 cells, while they were decreased for injection with TU-177/HNF1A-AS1 cells (Fig. 5D-F). This indicated that HNF1A-AS1 could promote laryngeal tumor growth either by subcutaneous injection or by submucosal injection into the tongue of nude mice. Additionally, the nude mice injected with TU-686/shRNA-2048 cells submucosally into the tongue had more metastatic cervical lymph nodes compared with those injected with TU-686/sh-NC cells, while

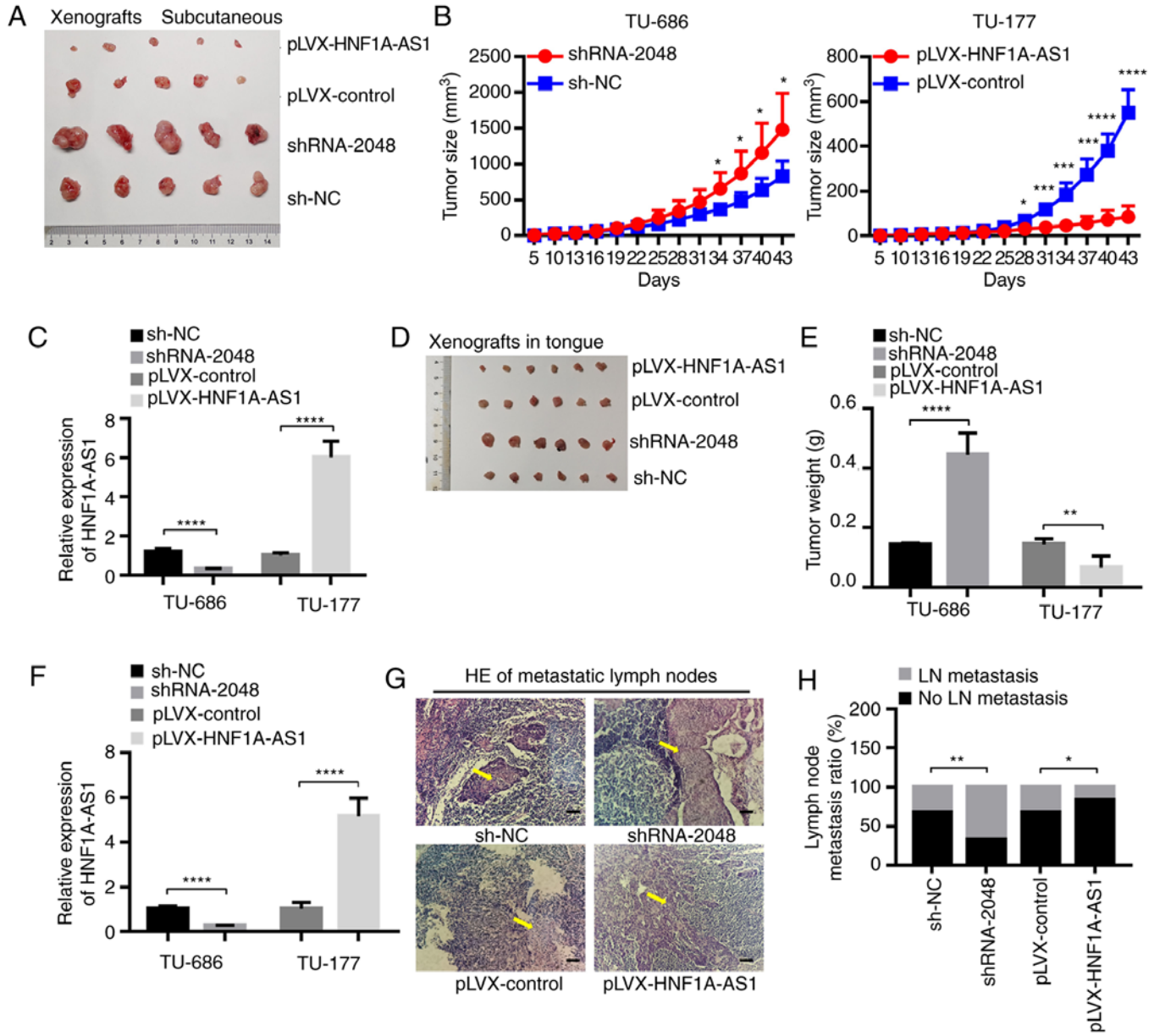

Figure 5. HNF1A-AS1 suppresses tumor growth and lymph node metastasis *in vivo*. (A) Typical specimens in the subcutaneous xenotransplant tumor model of human laryngeal cancer in nude mice. (B) Tumor growth curve and (C) RT-qPCR analysis of HNF1A-AS1 expression *in vivo* after the TU-686/shRNA-2048, TU-177/HNF1A-AS1 and control cells were injected subcutaneously into the right flank of nude mice (n=20). Tumor growth was calculated from day 5 and tumors were harvested from mice at 43 days after injection. (D) Typical specimens of tumors injected in tongues submucosally in the cervical lymph node metastasis model in nude mice. (E) Total weight of tumors submucosally injected into tongue of nude mice (n=24). (F) RT-qPCR analysis of HNF1A-AS1 expression. Tumors and cervical lymph nodes were harvested from mice at 15 days after injection. (G) Representative HE staining of cervical lymph node metastasis in HNF1A-AS1 knockdown or overexpression cells. Scale bar, 50 μm. Arrows indicate the metastasis in cervical lymph nodes. (H) Ratios of cervical lymph node metastasis in nude mice inoculated submucosally with the indicated cells into the tongue. Data are presented as the mean ± SD. All assays were performed in triplicate, and the values represent the mean of three independent experiments. For statistical analysis, an unpaired t-test was used. *P<0.05, **P<0.01, ***P<0.001, ****P<0.0001. The xenograft tumorigenicity experiment *in vivo* was performed one time. HNF1A-AS1, hepatic nuclear factor 1 α antisense RNA 1; NC, negative control; RT-qPCR, reverse transcription-quantitative PCR; shRNA, short hairpin RNA.

pathological examination confirmed the opposite effects for injection of TU-177/HNF1A-AS1 cells (Fig. 5G and H), demonstrating the inhibitory effect of HNF1A-AS1 on tumor lymph node metastasis. Furthermore, compared with that in the control group, E-cadherin expression was significantly downregulated, while Snail1, Slug, Vimentin and N-cadherin expression was significantly upregulated in tumors injected subcutaneously using TU-686/shRNA-2048 cells in nude mice according to western blotting and IHC. By contrast, upregulation of HNF1A-AS1 was associated with the opposite effects *in vivo* (Fig. 6). Collectively, these findings demonstrated that HNF1A-AS1 expression inhibited tumorigenic, as well as metastatic, abilities in a xenograft tumor model of nude mice via EMT.

Downregulation of HNF1A-AS1 is associated with hypermethylation of CpG island in promoter in vitro. To explore the inactivation mechanisms of HNF1A-AS1 in LSCC, the sequence of HNF1A-AS1 was analyzed and it was revealed that the promoter region of HNF1A-AS1 was rich in CpG

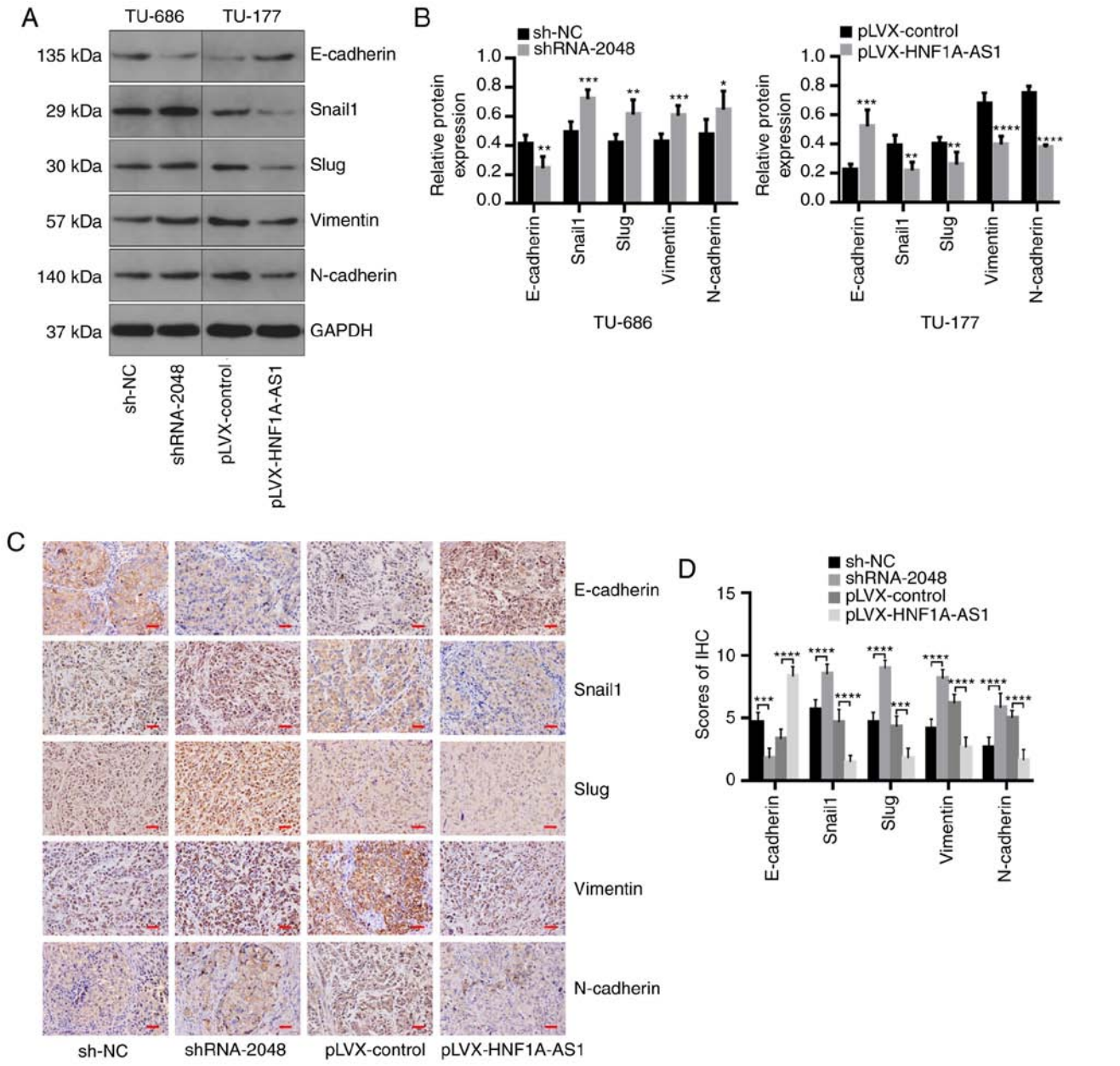

Figure 6. HNF1A-AS1 suppresses epithelial-mesenchymal transition *in vivo*. (A) Relative protein expression levels of E-cadherin, Snail1, Slug, Vimentin and N-cadherin in tumors in nude mice injected subcutaneously with TU-686/shRNA-2048, TU-177/HNF1A-AS1 and control cells were evaluated by western blot analysis, and (B) results of western blotting were analyzed statistically. (C) E-cadherin, Snail1, Slug, Vimentin and N-cadherin immunohistochemical staining in tumors in nude mice injected subcutaneously with the indicated cells, and (D) scores of IHC were a analyzed statistically. Scale bar, 25 μm. Data are presented as the mean ± SD. All assays were performed in triplicate, and the values represent the mean of three independent experiments. For statistical analysis, an unpaired t test was used for data in (B), and a χ^2 test was used for data in (D). *P<0.05, **P<0.01, ***P<0.001, ****P<0.0001. Western blotting and immunohistochemistry were performed in triplicate. HNF1A-AS1, hepatic nuclear factor 1 α antisense RNA 1; NC, negative control; shRNA, short hairpin RNA.

dinucleotides. The MethPrimer program was used to predict the distribution of CpG islands of HNF1A-AS1, and one CpG island (114 bp; -792 to -905 bp) was predicted within the promoter region of HNF1A-AS1 (Fig. 7A).

To clarify whether downregulation of HNF1A-AS1 was regulated by methylation in the CpG islands, TU-686 and TU-177 cells were treated with DNA methyltransferase inhibitor 5-Aza-dC, and the results demonstrated that the expression levels of HNF1A-AS1 were significantly increased in TU-686 and TU-177 cells following treatment with 5-Aza-dC at a dose of 5 and 10 μM for 48 h, revealing the crucial role of abnormal methylation in the inactivation of HNF1A-AS1 in LSCC cell lines (Fig. 7B).

Subsequently, a 148 bp segment in this region (-796 to -943 bp) that includes 7 CpG sites and spans the core promoter was analyzed using BSP (Fig. 7C). The hypermethylated CpG sites of TU-686 and TU-177 cells were 100 and 85.7%. Following treatment with 5 and 10 μM 5-Aza-dC, the hypermethylated CpG sites of TU-686 cells were decreased to 74.3 and 45.7%, respectively, and the ones of TU-177 cells were decreased to 71.4 and 31.4%, respectively (Fig. 7C). Similar to the BSP results, apparent methylation of HNF1A-AS1 in the promoter region was

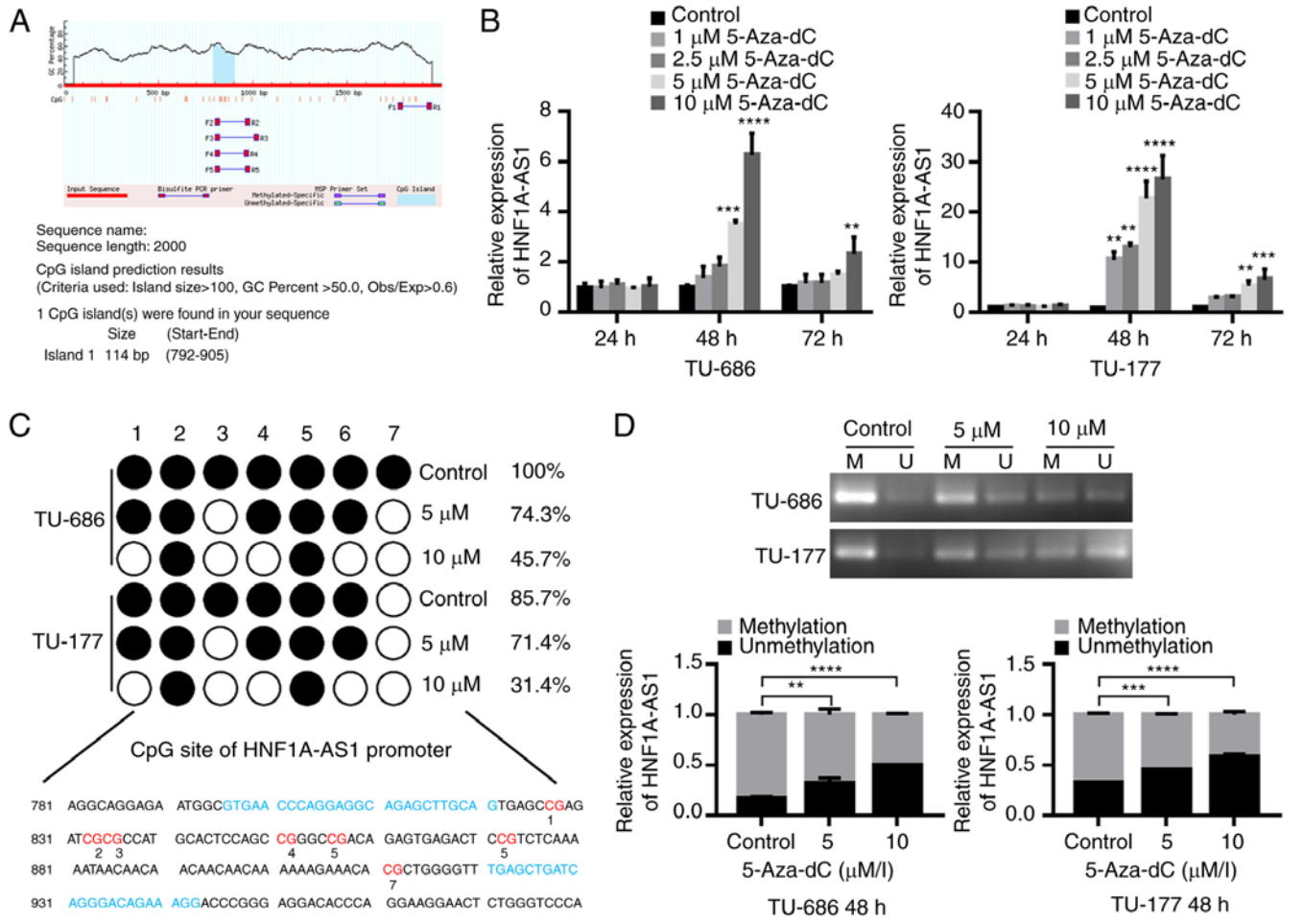

Figure 7. HNF1A-AS1 is downregulated due to promoter hypermethylation. (A) Bioinformatics analysis of CpG island in promoter region of HNF1A-AS1. (B) HNF1A-AS1 expression was increased following 5-Aza-dC treatment at different concentrations for 24, 48 and 72 h in TU-686 and TU-177 cells. (C) Methylation status of BSP for the HNF1A-AS1 CpG island in TU-686 and TU-177 cells treated with or without 5- Aza-dC after 48 h. White circle, unmethylated CpG dinucleotide; black circle, methylated CpG dinucleotide. (D) Methylation status of CpG island in HNF1A-AS1 promoter determined by MSP assay in TU-686 and TU-177 cells treated with or without 5-Aza-dC after 48 h. Data are presented as the mean ± SD. All assays were performed in triplicate, and the values represent the mean of three independent experiments. For statistical analysis, ANOVA with Tukey's post hoc test was used for data in (B and D) **P<0.01, ***P<0.001, ****P<0.0001. M, amplification with methylated primers; U, amplification with unmethylated primers; 5-Aza-dC, 5-Aza-2'-deoxycytidine; BSP, bisulfite genomic sequencing; HNF1A-AS1, hepatic nuclear factor 1 α antisense RNA 1; MSP, methylation-specific polymerase chain reaction.

also detected in TU-686 and TU-177 cells by MSP, in which the methylation status was partly reversed following 5-Aza-dC treatment. This revealed the importance of promoter methylation in the downregulation of HNF1A-AS1 expression (Fig. 7D).

Demethylation of CpG island in the promoter region of HNF1A-AS1 inhibits cell migration, invasion and EMT in vitro. The results demonstrated that the migration and invasion abilities of TU-686 and TU-177 cells were significantly decreased after demethylation of HNF1A-AS1 by 5-Aza-dC treatment (Fig. 8A-D). In addition, western blotting indicated that demethylation of the CpG island in the promoter of HNF1A-AS1 significantly upregulated E-cadherin expression and downregulated Snail1, Slug, Vimentin and N-cadherin expression (Fig. 8E and F). These data suggested that low HNF1A-AS1 expression which contributed to the invasion and metastasis of laryngeal cancer cells by affecting the EMT process may be the result of hypermethylation of HNF1A-AS1 in its promoter region.

Discussion

It is well recognized that enhanced proliferation, migration and invasion of LSCC cells serve key roles in the progression of LSCC (31,32). Therefore, the present study first determined that HNF1A-AS1 expression was low in human primary LSCC tissues and metastatic cervical lymph nodes compared with that in the adjacent non-tumor tissues. Due to the limitations of the difficulty in identifying targets that have low DNA and RNA copies, poor reproducibility and high expenses of *in situ* hybridization assays (33), RT-qPCR, which has been considered to be a reliable method for quantification of gene expression due to its accuracy, sensitivity, specificity and reproducibility (34), was used to assess the expression levels of HNF1A-AS1.

The present data demonstrated that HNF1A-AS1 decreased cell migration and invasive abilities *in vitro*, and reduced tumorigenesis and metastasis of xenograft LSCC tumors *in vivo*. The present study used a reduced concentration (1%) of serum to control for the influence of proliferation and avoid apoptosis

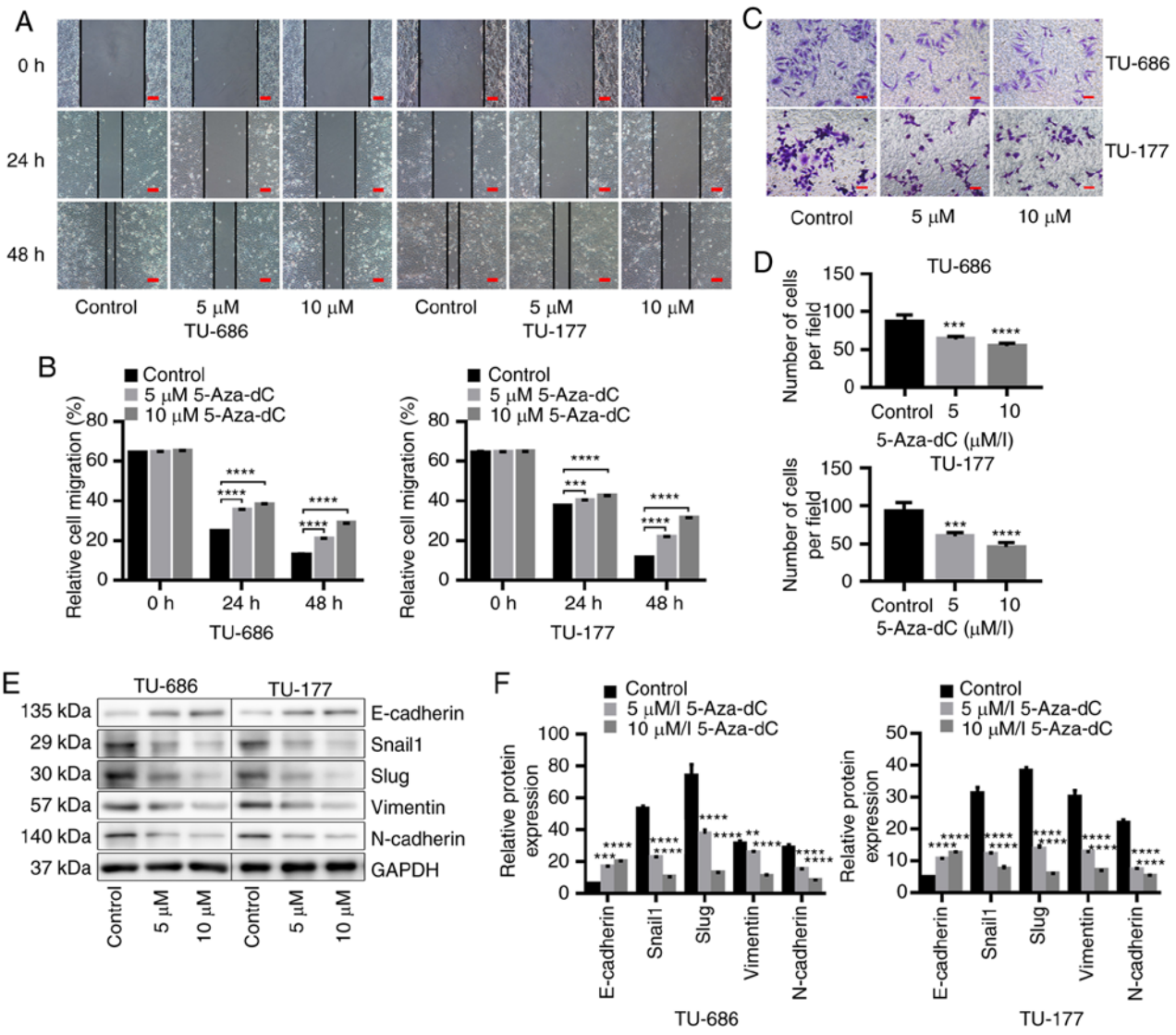

Figure 8. Demethylation of HNF1A-AS1 inhibits cell migration, invasion and epithelial-mesenchymal transition *in vitro*. (A) Cell migration abilities were tested using a scratch assay and (B) results of migration assays were analyzed statistically. Scale bar, 100 μm. (C) Invasive abilities were determined using a Transwell invasion assay in TU-686 and TU-177 cells treated with or without 5-Aza-dC after 48 h, and (D) the results of Transwell invasion assays were analyzed statistically. Scale bar, 50 μm. (E) Relative protein expression levels of E-cadherin, Snail1, Slug, Vimentin and N-cadherin were evaluated by western blot analysis in TU-686 and TU-177 cells treated with or without 5-Aza-dC after 48 h, and (F) results of western blotting were analyzed statistically. Data are presented as the mean ± SD. All assays were performed in triplicate, and the values represent the mean of three independent experiments. For statistical analysis, an ANOVA with Tukey's post hoc test was used. **P<0.01, ***P<0.001, ****P<0.0001. 5-Aza-dC, 5-Aza-2'-deoxycytidine; HNF1A-AS1, hepatic nuclear factor 1 α antisense RNA 1.

instead of FBS-free medium in the cell migration assay. Serum starvation can elicit complex, unpredictable time-dependent and cell-type-dependent effects. Low serum concentrations in cell medium is the most common method to suppress cell proliferation in wound healing assays (35). The duration of serum starvation and the required serum concentrations need to be rigorously determined for each studied cell line. It is commonly assumed that serum-starved cells have reduced basal cellular activity (36), but serum starvation has also been referred to as an 'environmental stress' (37) and 'apoptotic trigger' (38), implying dynamism that does not entirely fit the idea of a passive entry into a dormant hypoactive state. It remains an open issue whether diversity observed in the presence of serum also exists when cells are serum-starved in serum-free medium. The discrepancy may be due to differences in media composition, since cells were grown in 10% FBS prior to serum starvation.

Furthermore, according to the *in vitro* experiments, upregulation of HNF1A-AS1 led to proliferative inhibition by inducing G_0/G_1 phase cell cycle arrest in LSCC cells, while overexpression of HNF1A-AS1 significantly inhibited the protein expression of cyclin D1 and PCNA. Therefore, these findings suggested that HNF1A-AS1 may be a suppressor and serves an important role in the development and progression of LSCC.

EMT increases the invasive and metastatic capabilities of malignant tumor cells (7). Various epithelial-related proteins are involved in the EMT process, in which E-cadherin is implicated in transcriptional suppression, and vimentin is implicated in activation, leading to tumor invasion and metastasis (39). To investigate the probable underlying mechanisms, it was revealed that the expression levels of EMT-associated molecular markers (Snail1, Slug, Vimentin and N-cadherin) were decreased and E-cadherin remained high when HNF1A-AS1

was overexpressed in the laryngeal cells and xenografts, and vice versa when HNF1A-AS1 was downregulated. Overall, these findings indicated that LSCC tissues and laryngeal cancer cells with downregulated HNF1A-AS1 expression might undergo the EMT process, becoming more mobile and invasive, which promotes the malignant progression of LSCC.

As described in several studies (40,41), cancer cells often have a gain of methylation in the promoter regions of selected CpG islands, resulting in silencing of hundreds of genes, including tumor suppressor genes (42). In the present study, a CpG island was found in the promoter region of HNF1A-AS1, and the analysis using TCGA demonstrated that the methylation frequency in the promoter region of HNF1A-AS1 in HNSCC tissues was significantly higher than that in the corresponding normal tissues. According to the BSP and MSP results, CpG methylation of the HNF1A-AS1 promoter was detected in all primary LSCC tissues. Furthermore, a significantly different methylation status was identified among the metastatic cervical lymph nodes, cancer tissues and corresponding normal control tissues. This demonstrated that HNF1A-AS1 was downregulated in metastatic cervical lymph nodes and LSCC by hypermethylation On the other hand, the relationship between loss of HNF1A-AS1 expression and methylation of HNF1A-AS1 in LSCC cell lines was confirmed by excellent uniformity among mRNA expression by RT-qPCR, and DNA methylation in HNF1A-AS1 promoter by BSP and MSP, which largely accounted for the decreased expression levels of HNF1A-AS1. Additionally, following treatment with DNA methyltransferase inhibitor 5-Aza-dC, methylation of HNF1A-AS1 in TU-686 and TU-177 cells was reduced significantly, and the expression levels of HNF1A-AS1 were negatively associated with the methylation status. The migration, invasive abilities and EMT-associated marker expression in LSCC cell lines were reversed by treatment with 5-Aza-dC, which indicated that HNF1A-AS1 may act as a tumor suppressor lncRNA by regulating the EMT process via hypermethylation in LSCC.

However, the present study had some limitations, such as that the number of specimens was not sufficient to analyze the differences of prognosis and staging between HNF1A-AS1 high expression/hypermethylation and low expression/hypomethylation in patients with LSCC. Further studies on the overall survival information and deep functional investigations are required.

It is known that the expression of lncRNAs is strikingly cell type- and tissue-specific (10). Dang *et al* (15) reported that HNF1A-AS1 is downregulated in both gastric cancer tissues and cell lines. However, in a recent study, HNF1A-AS1 was demonstrated to inhibit the malignant properties of hepatocellular carcinoma cells both *in vitro* and *in vivo* (16). It is difficult to explain such phenomena; one possible explanation could be the heterogeneity of primary tumors. It was hypothesized that HNF1A-AS1 has a two-way regulatory role in different organs and carcinomas. More investigations are required to investigate this. Additionally, to the best of our knowledge, the expression and function of HNF1-AS1 and its methylation condition have not been reported in the development and progression of LSCC. In the present study, HNF1A-AS1 was downregulated by hypermethylation in LSCC and laryngeal cancer cells, and it served as a tumor suppressor lncRNA in LSCC by inducing the EMT process. These findings imply that manipulation of HNF1A-AS1 expression may have therapeutic effects against LSCC.

Acknowledgements

Not applicable.

Funding

The present study was supported by the National Natural Science Foundation of China (grant no. 81402246), Innovation Capability Support Program of Shaanxi (grant no. 2017KJXX-45), Natural Science Basic Research Program of Shaanxi (grant no. 2018JM7023), Natural Science Foundation Group-style Aided Tibet Medical Project of Tibet Autonomous Region [grant no. XZ2019ZR-ZY72 (Z)], Key Research and Development Program in Social Development Field of Shaanxi (grant no. 2019SF-084), and Special Research Fund for Talents Training in the Second Affiliated Hospital of Xi'an Jiaotong University [grant no. RC (GG) 201707].

Availability of data and materials

The datasets used and/or analyzed during the current study are available from the corresponding author on reasonable request.

Authors' contributions

YS performed the majority of the experiments, wrote the original draft, and was responsible for conceptualization and data curation. QZ, as the co-first author, performed some experiments and performed data visualization and analysis. MX and YF assembled the figures and resources, and collected samples. SM and CY performed formal analysis and visualization. ZW and YL performed the investigation. Acquisition of data, statistical analysis of the data and revision of the manuscript were performed by XL, HLi and HY. Parts of the cell and animal experiments were performed by HLi, YY and YZ, and they were also involved in drafting of the manuscript. The corresponding authors, XR and HLu, were major contributors in funding acquisition, designed experiments, and were involved in manuscript review and editing. All authors agreed to be accountable for all aspects of the work in ensuring that questions related to the accuracy or integrity of any part of the work are appropriately investigated and resolved. All authors read and approved the final manuscript.

Ethics approval and consent to participate

All patients provided written informed consent. The study was performed in accordance with the Declaration of Helsinki and was approved by the Ethics Committee of the Second Affiliated Hospital of Xi'an Jiaotong University (approval no. 2014001). All animal experiments were performed according to the Guide for the Care and Use of Laboratory Animals of the National Institutes of Health, and were subjected and approved by the Ethics Committee of Xi'an Jiaotong University (approval no. AE201812-01).

Patient consent for publication

Not applicable.

Competing interests

The authors declare that they have no competing interests.

References

1. Lee KW, Kuo WR, Tsai SM, Wu DC, Wang WM, Fang FM, Chiang FY, Ho KY, Wang LF, Tai CF, *et al*: Different impact from betel quid, alcohol and cigarette: risk factors for pharyngeal and laryngeal cancer. Int J Cancer 117: 831-836, 2005.
2. Muscat JE and Wynder EL: Tobacco, alcohol, asbestos, and occupational risk factors for laryngeal cancer. Cancer 69: 2244-2251, 1992.
3. Shen Z, Hao W, Zhou C, Deng H, Ye D, Li Q, Lin L, Cao B and Guo J: Long non-coding RNA AC026166.2-001 inhibits cell proliferation and migration in laryngeal squamous cell carcinoma by regulating the miR-24-3p/p27 axis. Sci Rep 8: 3375, 2018.
4. Rothenberg SM and Ellisen LW: The molecular pathogenesis of head and neck squamous cell carcinoma. J Clin Invest 122: 1951-1957, 2012.
5. Lefebvre JL, Coche-Dequeant B, Degardin M, Kara A, Mallet Y and Ton Van J: Treatment of laryngeal cancer: The permanent challenge. Expert Rev Anticancer Ther 4: 913-920, 2004.
6. Yang J and Weinberg RA: Epithelial-mesenchymal transition: At the crossroads of development and tumor metastasis. Dev Cell 14: 818-829, 2008.
7. Thiery JP, Acloque H, Huang RY and Nieto MA: Epithelial-mesenchymal transitions in development and disease. Cell 139: 871-890, 2009.
8. Perl AK, Wilgenbus P, Dahl U, Semb H and Christofori G: A causal role for E-cadherin in the transition from adenoma to carcinoma. Nature 392: 190-193, 1998.
9. Ponting CP, Oliver PL and Reik W: Evolution and functions of long noncoding RNAs. Cell 136: 629-641, 2009.
10. Ulitsky I and Bartel DP: lincRNAs: Genomics, evolution, and mechanisms. Cell 154: 26-46, 2013.
11. Batista PJ and Chang HY: Long noncoding RNAs: Cellular address codes in development and disease. Cell 152: 1298-1307, 2013.
12. Prensner JR and Chinnaiyan AM: The emergence of lncRNAs in cancer biology. Cancer Discov 1: 391-407, 2011.
13. Zou AE, Zheng H, Saad MA, Rahimy M, Ku J, Kuo SZ, Honda TK, Wang-Rodriguez J, Xuan Y, Korrapati A, *et al*: The non-coding landscape of head and neck squamous cell carcinoma. Oncotarget 7: 51211-51222, 2016.
14. Yang X, Song JH, Cheng Y, Wu W, Bhagat T, Yu Y, Abraham JM, Ibrahim S, Ravich W, Roland BC, *et al*: Long non-coding RNA HNF1A-AS1 regulates proliferation and migration in oesophageal adenocarcinoma cells. Gut 63: 881-890, 2014.
15. Dang Y, Lan F, Ouyang X, Wang K, Lin Y, Yu Y, Wang L, Wang Y and Huang Q: Expression and clinical significance of long non-coding RNA HNF1A-AS1 in human gastric cancer. World J Surg Oncol 13: 302, 2015.
16. Ding CH, Yin C, Chen SJ, Wen LZ, Ding K, Lei SJ, Liu JP, Wang J, Chen KX, Jiang HL, *et al*: The HNF1α-regulated lncRNA HNF1A-AS1 reverses the malignancy of hepatocellular carcinoma by enhancing the phosphatase activity of SHP-1. Mol Cancer 17: 63, 2018.
17. Subhash S, Andersson PO, Kosalai ST, Kanduri C and Kanduri M: Global DNA methylation profiling reveals new insights into epigenetically deregulated protein coding and long noncoding RNAs in CLL. Clin Epigenetics 8: 106, 2016.
18. Yan X, Hu Z, Feng Y, Hu X, Yuan J, Zhao SD, Zhang Y, Yang L, Shan W, He Q, *et al*: Comprehensive genomic characterization of long non-coding RNAs across human cancers. Cancer Cell 28: 529-540, 2015.
19. Sanger F, Nicklen S and Coulson AR: DNA sequencing with chain-terminating inhibitors. Proc Natl Acad Sci USA 74: 5463-5467, 1977.
20. Tong YS, Wang XW, Zhou XL, Liu ZH, Yang TX, Shi WH, Xie HW, Lv J, Wu QQ and Cao XF: Identification of the long non-coding RNA POU3F3 in plasma as a novel biomarker for diagnosis of esophageal squamous cell carcinoma. Mol Cancer 14: 3, 2015.
21. Zhou H, Wang F, Chen H, Tan Q, Qiu S, Chen S, Jing W, Yu M, Liang C, Ye S and Tu J: Increased expression of long-noncoding RNA ZFAS1 is associated with epithelial-mesenchymal transition of gastric cancer. Aging (Albany NY) 8: 2023-2038, 2016.
22. Livak KJ and Schmittgen TD: Analysis of relative gene expression data using real-time quantitative PCR and the 2(-Delta Delta C(T)) method. Methods 25: 402-408, 2001.
23. Aloysius MM, Zaitoun AM, Bates TE, Ilyas M, Constantin-Teodosiu D, Rowlands BJ and Lobo DN: Immunohistochemical expression of mitochondrial membrane complexes (MMCs) I, III, IV and V in malignant and benign periampullary epithelium: A potential target for drug therapy of periampullary cancer? BMC Cancer 10: 80, 2010.
24. Soslow RA, Dannenberg AJ, Rush D, Woerner BM, Khan KN, Masferrer J and Koki AT: COX-2 is expressed in human pulmonary, colonic, and mammary tumors. Cancer 89: 2637-2645, 2000.
25. Li LC and Dahiya R: MethPrimer: Designing primers for methylation PCRs. Bioinformatics 18: 1427-1431, 2002.
26. Du P, Zhang X, Huang CC, Jafari N, Kibbe WA, Hou L and Lin SM: Comparison of Beta-value and M-value methods for quantifying methylation levels by microarray analysis. BMC Bioinformatics 11: 587, 2010.
27. Council NR: Guide for the Care and Use of Laboratory Animals: Eighth edition. National Academies Press, Washington, DC, 2011. https://www.ncbi.nlm.nih.gov/books/NBK54050/. Accesion date April 2018.
28. Myers JN, Holsinger FC, Jasser SA, Bekele BN and Fidler IJ: An orthotopic nude mouse model of oral tongue squamous cell carcinoma. Clin Cancer Res 8: 293-298, 2002.
29. Sano D and Myers JN: Xenograft models of head and neck cancers. Head Neck Oncol 1: 32, 2009.
30. Chen LW, Wang JL, Zhang LY, Yang SM, Li CS, Yu N, Zhao WJD, Zhao LD, Li K, Liu MB and Zhai SQ: Establishment of an animal model of spontaneous cervical lymph node metastasis of laryngeal squamous cell carcinoma and obtaining laryngocarcinoma cells with high metastatic potential. Neoplasma 60: 504-510, 2013.
31. Li P, Yang Y, Liu H, Yang AK, Di JM, Tan GM, Wang HF, Qiu JG, Zhang WJ, Jiang QW, *et al*: MiR-194 functions as a tumor suppressor in laryngeal squamous cell carcinoma by targeting Wee1. J Hematol Oncol 10: 32, 2017.
32. Meng W, Cui W, Zhao L, Chi W, Cao H and Wang B: Aberrant methylation and downregulation of ZNF667-AS1 and ZNF667 promote the malignant progression of laryngeal squamous cell carcinoma. J Biomed Sci 26: 13, 2019.
33. Jensen E: Technical review: In situ hybridization. Anat Rec (Hoboken) 297: 1349-1353, 2014.
34. Sanders R, Mason DJ, Foy CA and Huggett JF: Considerations for accurate gene expression measurement by reverse transcription quantitative PCR when analysing clinical samples. Anal Bioanal Chem 406: 6471-6483, 2014.
35. Grada A, Otero-Vinas M, Prieto-Castrillo F, Obagi Z and Falanga V: Research techniques made simple: Analysis of collective cell migration using the wound healing assay. J Invest Dermatol 137: e11-e16, 2017.
36. Codeluppi S, Gregory EN, Kjell J, Wigerblad G, Olson L and Svensson CI: Influence of rat substrain and growth conditions on the characteristics of primary cultures of adult rat spinal cord astrocytes. J Neurosci Methods 197: 118-127, 2011.
37. Liu HS, Hsu PY, Lai MD, Chang HY, Ho CL, Cheng HL, Chen HT, Lin YJ, Wu TJ, Tzai TS and Chow NH: An unusual function of RON receptor tyrosine kinase as a transcriptional regulator in cooperation with EGFR in human cancer cells. Carcinogenesis 31: 1456-1464, 2010.
38. Bousette N, Chugh S, Fong V, Isserlin R, Kim KH, Volchuk A, Backx PH, Liu P, Kislinger T, MacLennan DH, *et al*: Constitutively active calcineurin induces cardiac endoplasmic reticulum stress and protects against apoptosis that is mediated by alpha-crystallin-B. Proc Natl Acad Sci USA 107: 18481-18486, 2010.
39. Kalluri R and Weinberg RA: The basics of epithelial-mesenchymal transition. J Clin Invest 119: 1420-1428, 2009.
40. Ehrlich M: DNA hypomethylation in cancer cells. Epigenomics 1: 239-259, 2009.
41. Tycko B: Epigenetic gene silencing in cancer. J Clin Invest 105: 401-407, 2000.
42. Herman JG and Baylin SB: Gene silencing in cancer in association with promoter hypermethylation. N Engl J Med 349: 2042-2054, 2003.